CrystEngComm

RSC Publishing

PAPER

Optical and structural characterization of N-face GaN epilayers grown on Ge (111) by plasma assisted molecular beam epitaxy

Cite this: *CrystEngComm*, 2013, **15**, 10590

Liyang Zhang,[ab] Ruben R. Lieten,*[ab] Tongtong Zhu,[c] Maarten Leys,[b] Sijia Jiang[b] and Gustaaf Borghs[ab]

Received 11th September 2013,
Accepted 9th October 2013

DOI: 10.1039/c3ce41836g

www.rsc.org/crystengcomm

The luminescence properties of N-face GaN, heteroepitaxially grown on Ge, is investigated and correlated with surface morphology and strain. The GaN surface shows a dense array of deep faceted pits at the end of threading dislocations. The density of defects increases with the epilayer thickness and relaxes the strain. GaN-on-Ge shows broad and intense photoluminescence, which exceeds the intensity of GaN grown on silicon, sapphire and SiC. Cathodoluminescence reveals the correlation of luminescence features with different crystal facets. Combined with the presence of impurity-induced band-tail states this leads to broad (330–410 nm) and intense optical spectra for N-face GaN-on-Ge.

Introduction

III-Nitrides semiconductors are widely studied due to their excellent performance in electronic and optoelectronic applications such as high electron mobility transistors (HEMTs) and light emitting diodes (LEDs). Traditionally, GaN layers are grown on sapphire substrates. However, using Si substrates one can realize low-cost manufacturing of GaN-based devices. For high performance, SiC substrates are used and also GaN wafers are available for homo-epitaxial growth. In the above mentioned cases, when foreign substrates are used, buffer layers inserted between the epitaxial layers and the substrate play a crucial role to circumvent the problems caused by the significant thermal and lattice mismatches between the GaN device layers and the substrate.[1]

For the fabrication of LEDs, a vertical device structure would be beneficial. A semiconductor substrate, which allows high quality GaN growth without intermediate layers, would be desired. Recently, the growth of GaN directly on Ge (111) substrates by plasma assisted molecular beam epitaxy (PA-MBE) has been reported and good GaN quality was achieved.[2,3] Although there is a large lattice mismatch of 20% and a thermal mismatch of −5.5% between GaN (0001) and Ge (111), structural characterization using cross-sectional transmission electron microscopy (TEM) shows that high quality GaN epilayers can be achieved when the GaN epilayers are grown on an off-axis substrate or at a relatively high temperature (HT).[4] In addition, using convergent beam electron diffraction (CBED), the GaN-on-Ge epilayers have been shown to have N-polarity.[4]

N-Polarity is interesting for GaN LED structures because it helps to suppress efficiency droop,[5,6] the phenomenon of reduced efficiency at high power. Besides N-polar LEDs,[5,6] several other approaches to suppress efficiency droop have been suggested, such as quantum barrier engineering method,[7–9] and large electron–hole wave function overlap quantum well (QW) approaches.[10–12]

Whilst the GaN grown on sapphire, Si, and SiC have been quite extensively studied, N-face GaN-on-Ge has received less attention, but nonetheless Ge may be considered as a promising substrate for optoelectronic applications. Therefore, the study of GaN-on-Ge is of importance both in view of better understanding of the GaN epitaxy as well as considering new commercial substrates. In this paper we further investigate the structural and optical properties of GaN epilayers grown on Ge (111) substrates by PA-MBE. Furthermore we investigate the emission of light by GaN-on-Ge.

Results and discussion

Sample fabrication

Ge (111) substrates are chemically cleaned to remove metallic contamination, particles and native oxide from the surface, just before loading into the MBE system. Subsequently the samples are degassed at 450 °C in vacuum with a background pressure of 1×10^{-9} Torr. The cleanliness of the surface is confirmed by reflection high energy electron diffraction

[a] *Department of Physics and Astronomy, K. U. Leuven, 3001 Leuven, Belgium. E-mail: Ruben.Lieten@gmail.com*
[b] *IMEC, Kapeldreef 75, 3001 Leuven, Belgium*
[c] *Department of Materials Science and Metallurgy, University of Cambridge, Pembroke Street CB2 3QZ, Cambridge, UK*

(RHEED), which shows a reconstructed surface. Substrate temperatures are measured by thermocouple. A N_2 flow of 0.6 standard cubic centimetres per minute (SCCM) and a radio frequency power of 250 W have been used. These settings correspond to a flux of around 3.2×10^{14} atoms cm^{-2} s^{-1}. After the formation of single crystalline Ge_3N_4 (only two monolayers thick),[13] by 1-minute nitrogen plasma exposure, the Ga shutter is opened and GaN growth is started under Ga-rich condition. A series of samples were directly grown on Ge (111) substrates at relatively HT of around 850 °C, with a Ga flux of 4.7×10^{-7} Torr and a N_2 flow of 0.6 sccm. Only the growth time was changed.

Structural characterization

The GaN epilayer thicknesses were measured by ellipsometry and are listed in Table 1, which also shows the surface roughness as determined by tapping mode atomic force microscopy (AFM), and the X-ray ω scan full width at half maximum (FWHM) of reflections α-GaN (0002) and (10$\bar{1}$2) and β-GaN (002).

With increasing layer thickness from 61 to 307 nm, both the root-mean-square (RMS) and peak-to-valley (P–V) roughness increase, see Table 1. As will be described below, the obtained surface roughness of sample A is partially due to the islands' texture. With a further increase in layer thickness to 1196 nm, the surface roughness decreases, and shows a convergence trend, as the surface roughness is similar for the 409 nm and 1196 nm thick samples.

The FWHM of X-ray ω scans follow a similar trend as the surface roughness: increases for increasing GaN layer thickness from 61 to 307 nm and then decreases for thicker layers. This result hints that surface roughness depends on material quality. Additionally, according to the X-ray diffraction (XRD) φ scans, cubic GaN inclusions exist for all the samples (not shown). These cubic inclusions, also referred to as β-GaN are oriented with the (111) planes parallel to the α-GaN (0001) planes.[14]

Distinctive surface morphologies are observed by scanning electron microscopy (SEM) and AFM as shown in Fig. 1. The surface morphological features are linked to the GaN polarity for Ga-rich growth: it has been reported that the epitaxy of GaN layers with N face leads to rougher surfaces than for Ga face.[15–18] High angle annular dark field scanning transmission electron microscopy (HAADF-STEM) measurements were

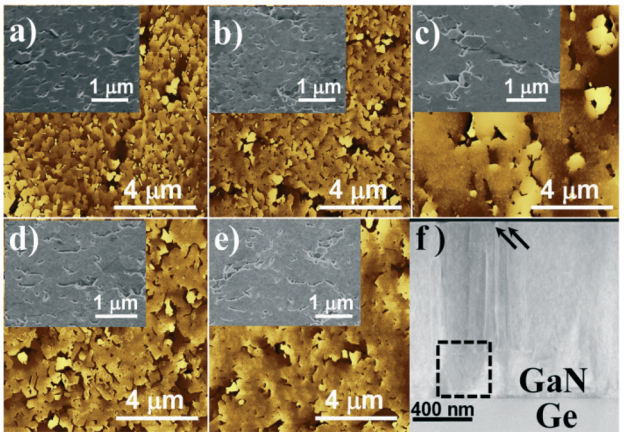

Fig. 1 (a)–(e) AFM profiles with scan size of 10 μm × 10 μm for sample A to E with SEM profiles inset, and (f) is the HAADF-STEM image of sample E. The arrows show the pits at the end of the threading dislocations, and dotted rectangle shows the grains.

employed to study the structural properties of GaN-on-Ge, see Fig. 1(f). The GaN epilayers' surfaces show deep faceted pits at the end of threading dislocations. For MBE growth near stoichiometric conditions, the growth rate of N-face domains may be slightly lower than that of Ga-face matrix, leading to the formation of pits with inversion domains at their centers.[7] Thus, we conclude that faceted surface follows from the N-face polarity of GaN epilayers on Ge substrates.

For sample A, the GaN epilayer shows a grainy appearance due to slight misorientations induced by the vertical defects as indicated by both AFM and TEM. Small GaN grains are observed for the thin layer, while the grains become larger for increasing thickness and the grains coalesce for the thicker layers. Small-angle grain boundaries are probably formed with clustering of threading dislocations. For sample E, TEM indicates that the columnar structure causes both "tilt" and "twist" of the islands with respect to each other due to threading dislocations in the GaN layer. In all cases, an array of threading dislocations is found at the boundaries. In addition, for this sample a layer with "grains" with a higher defect density can be distinguished at the bottom of the GaN layer near the interface as identified by the dotted rectangle shown in Fig. 1(f). Growth of these grains in different directions therefore can give rise to faceted GaN epilayer surfaces. Based on TEM, more defects are visible for thick samples, which is correlated with a strain relaxation mechanism.[19]

Table 1 Properties of GaN epilayers: thickness, RMS and P–V surface roughness, FWHM of X-ray ω scan, lattice constants, and *c*-axis strain

Sample no.	Thickness (nm)	RMS (nm)	P–V (nm)	FWHM (arcsec) α-GaN (0002)	FWHM (arcsec) α-GaN 10$\bar{1}$2	FWHM (arcsec) β-GaN (002)	Lattice constant *c* (Å)	Lattice constant *a* (Å)	$\varepsilon_\perp$ (10^{-4})
A	61	8.4	257	410	1116	1224	5.1872	3.1810	4.3
B	145	12.2	295	612	1260	1296	5.1863	3.1842	2.4
C	307	19.4	330	626	1764	2232	5.1850	3.1883	0.06
D	409	10.6	225	544	1188	2088	5.1852	3.1877	0.41
E	1196	8.6	204	536	1332	2736	5.1850	3.1885	−0.06

The lattice constants can be determined by high-resolution XRD scans as shown in Fig. 2, and consequently also strain. We measured the out-of-plane c lattice spacing from the (0002) GaN reflection, as listed in Table 1. From ref. 20, lattice constant a can be derived from c by

$$a = a_0 - \frac{a_0(c - c_0)}{c_0 \nu} \quad (1)$$

where c_0 = 5.1850 and a_0 = 3.1884 are the lattice constant of unstrained GaN, and ν = 0.183 is the Poisson ratio of bulk GaN.[21]

A theoretical equation to fit the lattice constant a as function of layer thickness was used to derive the critical thickness. This equation is expressed by[20]

$$a = a_0 + \frac{h_c}{h}(a_s - a_0) \quad (2)$$

where h_c and h are the critical thickness and the thickness of the epilayer, respectively. a_s is the lattice constant of the substrate. The lattice constant of substrate a_s of 3.1751 Å and the critical thickness h_c of 34 nm were obtained to fit our data in the whole region of the thickness. The critical thickness of 34 nm is in a good agreement with the one of 29 nm of GaN films on sapphire substrates.[20] As mentioned before, two monolayer thick Ge_3N_4 is formed during growth and GaN for a small thickness grows coherently on this template. We, therefore, attribute the a_s of 3.1751 Å to the interface layer Ge_3N_4.

Normally, the total strain consists of intrinsic growth strain and extrinsic thermal strain. The degree of strain relaxation will depend on the layer thickness. The lattice constants of all samples were determined by HR-XRD scans and then the total strain was deduced. Based on eqn (1) and (2), we can obtain the a-axis and c-axis strain as:

$$\varepsilon_{\parallel} = \frac{a - a_0}{a_0} = \frac{h_c(a_s - a_0)}{h a_0} \quad (3)$$

$$\varepsilon_{\perp} = -\upsilon \varepsilon_{\parallel} \quad (4)$$

When the GaN epilayer thickness is below the critical thickness of 34 nm, the GaN layer is expected to have the same in-plane lattice spacing of the growth template, indicating a constant strain of -4.2×10^{-3} in a-plane, and of 7.6×10^{-4} in c-plane. While the GaN epilayer thickness is beyond 34 nm, the strain relaxes for increasing thickness.

In addition, our measurements show that the strain relaxes exponentially as function of GaN layer thickness as described by the expression in the inset of Fig. 3, which shows the variations of the c-axis strain (ε_c) and the dominant photoluminescence (PL) energetic positions of the GaN-on-Ge as function of the layer thickness. The parameter ε_c^0 is the initial strain and the parameter L is the relaxation depth at which the strain relaxes to 1/e of the initial strain.[22] The relaxation depth L depends on the substrate and layer properties. The evolution of lattice spacing as function of layer thickness was fitted using an initial strain of 7.3×10^{-4}, and a relaxation depth of 118 nm. The strain therefore relaxes to 37% (1/e), 5%, 1% for a layer thickness of 118 nm, 353 nm and 543 nm, respectively.

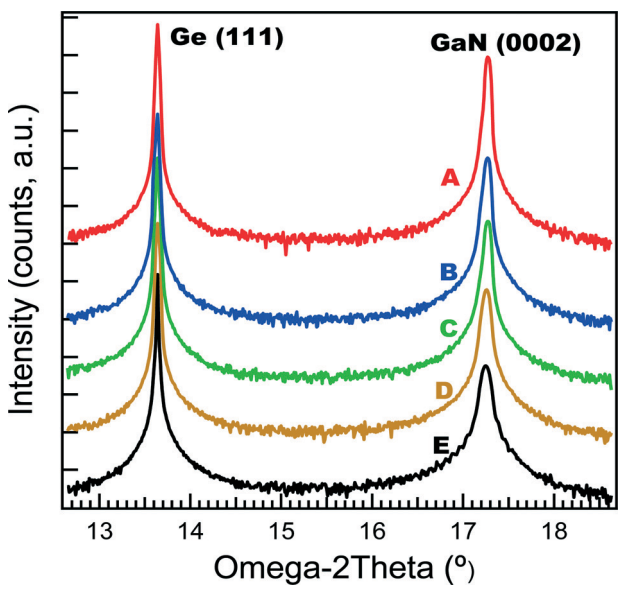

Fig. 2 The high-resolution XRD ω-2θ scans. Each HR-XRD scan includes the substrate Ge (111) peak, which is used as calibration reference for the position of the GaN (0002) peak.

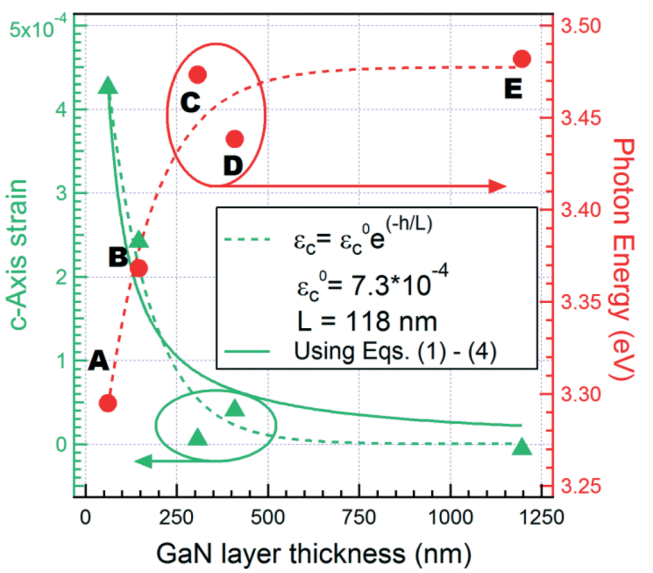

Fig. 3 c-Axis strain and PL emission energy of the GaN epilayers as function of the layer thickness. The dashed line of PL emission energy (red) is a guide to the eye. The c-axis strain relaxation is fitted by an exponential curve (green dashed line) and the fitting parameters are shown in the figure. The solid line (green) is the c-axis strain derived from eqn (1)–(4).

The initial strain of 7.3×10^{-4} is in good agreement with the one of 7.6×10^{-4}, which is derived from the "critical thickness" model. The calculated *c*-axis strain, as a function of the layer thickness by using eqn (1)–(4), is shown in Fig. 3 (solid curve). The strain difference between this model and the real strain can be explained by the fact that most relaxation occurs *via* surface roughening/faceting for thick layers.

Optical characterization

With increasing GaN epilayer thickness, the strain changes and this has a pronounced impact on the optical properties of GaN-on-Ge. PL measurements were performed with a 325 nm HeCd laser (10 mW nominal optical power) employed as the excitation source. Differences in the strain change the bandgap and shift the PL peak positions.[23] With increasing layer thickness, the strain relaxes and tends to be zero (-1.3×10^{-6}) at a thickness of about 750 nm. Correspondingly, a blue shift in emission energy (from 3.295 eV to 3.4818 eV) is observed when going from sample A to E as shown in Fig. 3. The dominant energetic positions were obtained from the Gaussian fitting of the spectra in Fig. 4(a).

Room temperature (RT) PL spectra of all the samples of GaN grown on Ge (111) are displayed in Fig. 4(a). The line widths of sample A and B are around 210 meV, while the line widths of sample C, D, and E are around 135 meV. Except for the thick sample E, only one broad dominant peak is resolvable for samples A to D.

Absorption in the visible spectrum by the Ge substrate has to be suppressed for vertical III-nitride-on-Ge devices. This concern is similar to the case of GaN-on-Si, for which the wafer can be bonded on a surrogate substrate and the Si substrate removed by wet-chemical etching. Several possible approaches for Ge are suggested: (1) wafer bonding and removal of the Ge substrate (1) wafer bonding and thinning of the Ge substrate followed by local removal of the Ge substrate to open an optical window. (3) Insertion of a reflection layer between the Ge substrate and QWs. (4) Improving the reflection of Ge by doping and using the Ge as reflection layer.

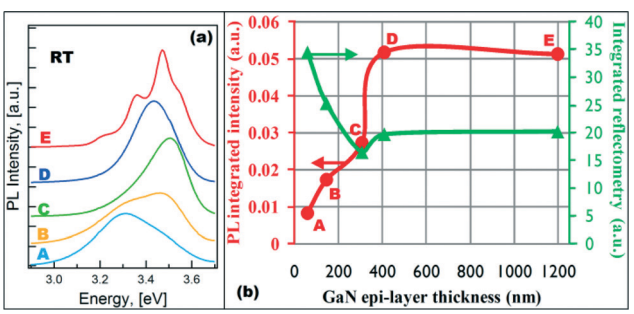

Fig. 4 (a) PL spectra of all the samples at RT. PL spectra were normalized by each PL integrated intensity over the energy scan region and vertically shift. (b) PL and integrated reflection as function of GaN epilayer thickness. Firstly, the PL intensity increases with thickness due to the absorption depth. At the same time, the extraction increases because of the increased roughness (decreased reflectivity) and then it saturates because the reflectivity saturates. The surface recombination seems to be low for sample D and E.

The PL integrated intensity as function of the GaN epilayer thickness is shown in Fig. 4(b). The PL integrated intensity strongly increases for increasing layer thickness from 60 nm to ~400 nm and then nearly saturates when the layer thickness increases to ~1200 nm. For the PL excitation source used in this work (3.81 eV), the penetration depth is estimated to be ~100 nm. Thus, full absorption in sample A is not achieved. The limited thickness combined with the island texture for sample A also leads to more non-radiative surface recombination. In other samples the absorption is assumed to be complete.

The GaN surface morphology and structural quality strongly affect the optical performance as well. As can be seen in Fig. 4(b), from sample A to B, an increase in PL intensity is observed. An increase in defects in the GaN epilayers would lead to a stronger non-radiative recombination and would result in a lower PL intensity. Thus, the increased non-radiative recombination of sample B is counteracted by other mechanisms. We propose the combined effect of an increase in absorption and enhanced extraction efficiency because of the increased roughness. This trend is continued with increased GaN thickness from sample B to C: the main reason of the increased intensity is due to an increase in the extraction efficiency (RMS roughness increases from 12.2 to 14.5 nm, P–V from 295 to 330 nm).

Additional optical reflectivity measurements were carried out to investigate the influence of sample morphology on light reflection. The observed integrated reflection intensity over the PL energy scan region (2.83 eV to 3.77 eV) is shown in Fig. 4(b). From sample A to C, the reflectivity decreases, corresponding to an increase in surface roughness. The reflectivity slightly increases from sample C to D, and then saturates with further increased layer thickness. Therefore, although the surfaces of thick samples (D and E) are smoother than the thin samples, the extraction ability is still strong for these two samples because of their surface texture (see Fig. 1).

The high PL intensities of sample D and E indicate that their surface non-radiative recombination is limited. The PL spectrum of sample E is compared with spectra of GaN grown on sapphire, Si, and SiC grown by metal organic vapor phase epitaxy (MOVPE) as shown in Fig. 5(a). All of these three samples are unintentionally doped (UID) and grown at HT. The growth details can be found in earlier work.[1] The layer thickness and the FWHM of XRD (thickness, (0002), ($10\bar{1}2$)) rocking curve of GaN on sapphire, Si and SiC are (3.3 μm, 219 arcsec, 304 arcsec), (2.3 μm, 473 arcsec, 429 arcsec) and (1.3 μm, 293 arcsec, 324 arcsec), respectively. Despite the defect density is larger in GaN-on-Ge as suggested by the FWHM's of XRD, the PL spectrum of GaN-on-Ge is much stronger and broader compared to the other spectra.

As mentioned above, the surface of these GaN-on-Ge epilayers are rough and with faceted pits. The surface

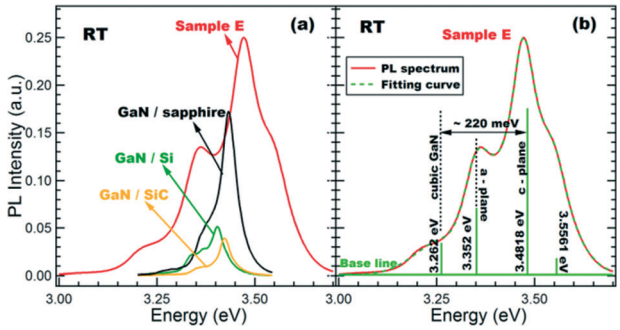

Fig. 5 (a) Near-bandgap PL spectra of GaN on Ge (sample E), sapphire, Si and SiC, respectively. (b) PL spectrum of sample E (solid line) was fitted with a multi-Gaussian function (dashed line). The fitted energetic positions and emission intensities (vertical solid lines) are shown.

morphology of the GaN-on-Ge layers is distinctive from GaN on sapphire, Si and SiC. Based on AFM measurements, the surfaces of GaN on sapphire, Si and SiC are quite smooth and P–V roughnesses are less than 20 nm. The morphology of sample E with P–V roughness above 200 nm as observed by AFM/SEM/TEM indicates that a natural photonic crystal was formed. This morphology helps to extract more light from the GaN epilayer due to the texturing of the surface, which leads to more reflection and extraction of light. It should be noted that the P–V values are influenced by the AFM tip size and are therefore indicative values. Longer effective lifetime of photo excited carriers might be an alternative explanation of the intense PL of N-face GaN.[24]

Earlier work shows that the PL line width increases monotonically with carrier concentration ($>10^{18}$ cm^{-3}) due to tailing of the density of states.[25] One may consider the influence of Ge atoms diffusion into the GaN layers during growth, as a higher n-type background impurity concentration is present in these GaN-on-Ge layers. For the case of UID GaN-on-Ge layers, secondary ion mass spectroscopy (SIMS) measurements in our previous work show high Ge content (in counts/s), indicating Ge concentration is as large as 1×10^{20} cm^{-3} assuming 100% activation.[6] So the influence of Ge atoms diffusion on the broadening PL cannot be ruled out because the carrier concentration level of 10^{20} cm^{-3} is already high enough to form a continuous band tail.

We propose here that the luminescence is correlated with the surface morphology in the case of GaN-on-Ge. As shown in Fig. 5(b), the PL spectrum of sample E can be fitted with a multi-Gaussian function, and four peaks are resolvable with the fitted energetic positions and emission intensities. As most of the light originates from *c*-plane GaN, as will be shown later by cathodoluminescence (CL) measurements, we assign the dominant peak at 3.4818 eV to *c*-planes. XRD measurements show that cubic GaN is present in our samples. The difference in bandgap energy between cubic and wurtzite GaN is around 210 meV.[26] Such energy difference is in a good agreement with the energy difference of 220 meV between the luminescence line in the left side and the dominant line as marked in the spectrum. We therefore assign it to emission from cubic GaN. The different PL transitions from different GaN facets are at different energetic positions due to different polarization fields in each facet.[27] The *a*-planes show a red shift in emission energy of 132 meV with respect to the luminescence from the *c*-planes.[28] Thus, the second line from the left side is distinguished from *a*-planes as the emission energy difference of 130 meV from the dominant line. The luminescence line at 3.5561 eV is around 74 meV higher than the dominant luminescence line, which exceeds the adopted value due to the effects of Burstein Moss shift (30 meV for carrier concentration of 3×10^{19} cm^{-3}).[29] We thus suggest several possibilities. One is that this line stems primarily from *c*-planes of a thicker region based on the following considerations. According to the images from TEM, the thickness of sample E is not uniform. With increasing epilayer thickness strain is relaxed and thereby induces emission blue shift. The other possibility could be due to the effect of the interface between GaN and Ge. During the growth, voids are present at the top of the Ge surface, resulting from Ge diffusion into the GaN.[30]

In addition, we have performed cathodoluminescence (CL) measurements at RT at 5 kV in a Philips XL30 equipped with a Gatan MonoCL4 system. The SEM image, the corresponding integrated CL-spectrum, and a set of monochromatic CL intensity images of sample E are shown in Fig. 6. The small difference between the integrated PL-spectrum (Fig. 5) and CL-spectrum is due to different scan areas.

Based on the monochromatic CL imaging of sample E, the surface morphology has a strong impact on the luminescence. The CL image at 3.471 eV displays a bright emission from most regions over the scan area, indicating the dominant peak at 3.471 eV is mostly from the $(000\bar{1})$ surface. The columnar structures, indicated by the circles, show higher CL intensity over a broad range of emission energies.

In order to distinguish the emission from different surface features, CL spectrum imaging (each pixel of the spectrum image contains a spectrum recorded by a charge coupled device camera) was performed over an area of 41 × 34 pixels with a step size of 35 nm (Fig. 7). CL spectra extracted from different positions of sample E are shown in Fig.7(d–i). Spot 1 is taken from the flat surface [Fig. 7(d)]. Despite the low

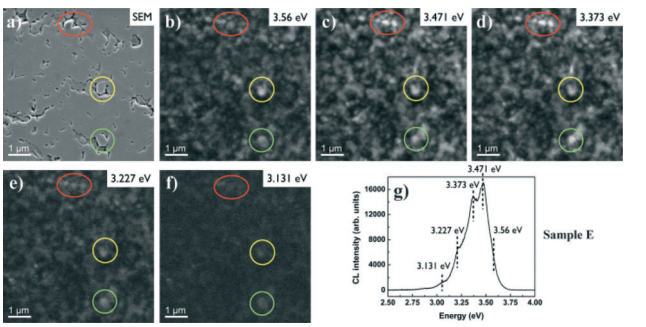

Fig. 6 a) SEM and monochromatic CL intensity images sample E at RT at b) 3.56 eV, c) 3.471 eV, d) 3.373 eV, e) 3.227 eV, and f) 3.131 eV. g) The integral CL-spectrum of sample E.

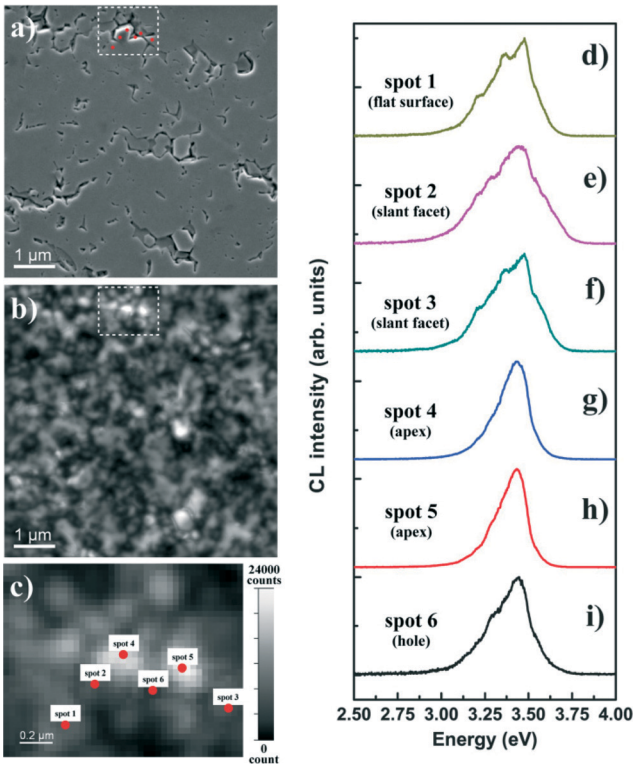

Fig. 7 a) SEM and b) panchromatic CL images of sample E. c) The corresponding CL spectrum image (a two-dimensional integrated CL intensity map, in which each pixel of the image contains a spectrum recorded by a charge coupled device camera) of sample E, CL spectra extracted from d) flat surface, e and f) slant facet, g and h) apex, i) hole as indicated by the red dots in the SEM and the CL spectrum image.

energy tail, it shows a strong steep high-energy cut-off of the emission at 3.471 eV. Spot 2 and 3 are taken from slant facets and show a very broad band from 2.9–3.8 eV. Both spot 4 and 5 are from the apex of the surface feature and show an intense emission at 3.43 eV. Spot 6 is from a hole with different facets and shows a similar broad band but with much less intensity, which is probably due to difference in local light extraction efficiency or the presence of defects.

For both the PL (Fig. 5) and CL (Fig. 6) spectra of sample E, different energetic positions with various intensities are obtained in the integrated spectra for a given scan area. The origin of each peak has been explained above and has been indicated in Fig. 5(b). Fig. 7, which shows the local CL spectra, confirms this explanation. For different locations, the CL shows a shift in peak energy. These observations suggest that the surface morphology strongly influences the luminescence properties due to a difference in polarization field for each facet and differences in material quality.

Conclusions

In conclusion, the luminescence properties of N-face GaN epilayers on Ge (111) substrates have been investigated and have been correlated with structural properties. The thickness of GaN epilayers influences the sample's surface morphology, optical properties and strain. The strain in the GaN epilayer relaxes exponentially with increasing layer thickness, which leads to clear blue shift in emission energy. It has been shown that the faceted surface follows from the N-face polarity. The surface of these GaN epilayers shows faceted deep pits, which results in broad and strong emission as revealed by CL and PL. The intense PL from GaN-on-Ge layers exceeds the emission intensity of GaN grown on sapphire, Si, and SiC substrates.

Acknowledgements

R. R. L. acknowledges support as Research Fellow of the Research Foundation – Flanders (FWO). W. van de Graaf is acknowledged for assistance in epitaxial growth and X-ray diffraction. Paola Favia and Hugo Bender are acknowledged for assistance in the HAADF-STEM.

References

1 L. Zhang, K. Cheng, S. Degroote, M. Leys, M. Germain and G. Borghs, *J. Appl. Phys.*, 2010, **108**, 073522.
2 R. R. Lieten, S. Degroote, K. Cheng, M. Leys, M. Kuijk and G. Borghs, *Appl. Phys. Lett.*, 2006, **89**, 252118.
3 R. R. Lieten, S. Degroote, M. Leys and G. Borghs, *J. Cryst. Growth*, 2009, **311**, 1306.
4 Y. Zhang, W.-Y. Fu, C. Humphreys and R. R. Lieten, *Appl. Phys. Express*, 2011, **4**, 091001.
5 S. Keller, C. S. Suh, N. A. Fichtenbaum, M. Furukawa, R. Chu, Z. Chen, K. Vijayraghavan, S. Rajan, S. P. DenBaars, J. S. Speck and U. K. Mishra, *J. Appl. Phys.*, 2008, **104**, 093510.
6 F. Akyol, D. N. Nath, S. Krishnamoorthy, P. S. Park and S. Rajan, *Appl. Phys. Lett.*, 2012, **100**, 111118.
7 S. Choi, M.-H. Ji, J. Kim, H. J. Kim, M. M. Satter, P. D. Yoder, J.-H. Ryou, R. D. Dupuis, A. M. Fischer and F. A. Ponce, *Appl. Phys. Lett.*, 2012, **101**, 161110.
8 H. Zhao, X. Jiao and N. Tansu, *J. Disp. Technol.*, 2013, **9**, 212.
9 G. Y. Liu, J. Zhang, C. K. Tan and N. Tansu, *IEEE Photonics J.*, 2013, **5**, 2201011.
10 D. Feezell, J. Speck, S. DenBaars and Sh. Nakamura, *J. Disp. Technol.*, 2013, **9**, 190.
11 H. Zhao, G. Liu, J. Zhang, J. D. Poplawsky, V. Dierolf and N. Tansu, *Opt. Express*, 2011, **19**, A991.
12 R. A. Arif, Y.-K. Ee and N. Tansu, *Appl. Phys. Lett.*, 2007, **91**, 091110.
13 R. R. Lieten, O. Richard, S. Degroote, M. Leys, H. Bender and G. Borghs, *J. Cryst. Growth*, 2011, **314**, 71.
14 S. Oktyabrsky, K. Dovidenko, A. K. Sharma, J. Narayan and V. Joshkin, *Appl. Phys. Lett.*, 1999, **74**, 2465.
15 E. C. Piquette, P. M. Bridger, Z. Z. Bandic and T. C. McGill, *J. Vac. Sci. Technol., B*, 1999, **17**, 1241.
16 M. Seelmann-Eggebert, J. L. Weyher, H. Obloh, H. Zimmermann, A. Rar and S. Porowski, *Appl. Phys. Lett.*, 1997, **71**, 2635.

17 J. L. Rouviere, J. L. Weyher, M. Seelmann-Eggebert and S. Porowski, *Appl. Phys. Lett.*, 1998, **73**, 668.
18 B. Daudin, J. L. Rouviere and M. Arlery, *Appl. Phys. Lett.*, 1996, **69**, 2480.
19 H. K. Cho, J. Y. Lee, C. S. Kim, G. M. Yang, N. Sharma and C. Humphreys, *J. Cryst. Growth*, 2001, **231**, 466.
20 C. Kim, I. K. Robinson, J. Myoung, K. Shim, M.-C. Yoo and K. Kim, *Appl. Phys. Lett.*, 1996, **69**, 2358.
21 M. A. Moram, Z. H. Barber and C. J. Humphreys, *J. Appl. Phys.*, 2007, **102**, 023505.
22 W. J. Tseng, M. Gonzalez, L. Dillemans, K. Cheng, S. J. Jiang, P. M. Vereecken, G. Borghs and R. R. Lieten, *Appl. Phys. Lett.*, 2012, **101**, 253102.
23 H. Amano, K. Hiramatsu and I. Akasaki, *Jpn. J. Appl. Phys.*, 1988, **27**, L1384.
24 G. Tamulatis, I. Yilmaz, M. S. Shur, R. Gaska, C. Chen, J. Yang, E. Kuokstis, A. Khan, S. B. Schujman and L. J. Schowalter, *Appl. Phys. Lett.*, 2003, **83**, 3507.
25 E. Iliopoulos, D. Doppalapudi, H. M. Ng and H. D. Moustakas, *Appl. Phys. Lett.*, 1998, **73**, 375.
26 I. Vurgaftman and J. R. Meyer, *J. Appl. Phys.*, 2003, **94**, 3675.
27 L. Zhang, K. Cheng, M. Leys, P. Favia, H. Bender and G. Borghs, *J. Appl. Phys.*, 2011, **110**, 083518.
28 F. Bertram, J. Christen, M. Schmidt, M. Topf, S. Fischer and B. Meyer, *Mater. Sci. Eng., B*, 1997, **50**, 165.
29 R. D. Cunningham, R. W. Brander, N. D. Knee and D. K. Wickender, *J. Lumin.*, 1972, **5**, 21.
30 Y. Zhang, C. McAleese, H. Xiu, C. J. Humphreys, R. R. Lieten, S. Degroote and G. Borghs, *Phys. Status Solidi C*, 2008, **5**, 1802.

